Adsorption structure of adenine on cerium oxide

Sofiia Bercha¹, Suman Bhasker-Ranganath², Xiaohui Zheng³, Klára Beranová^{1,a}, Mykhailo Vorokhta¹, Robert G. Acres^{4,b}, Tomáš Skála¹, Vladimír Matolín¹, Kevin C. Prince⁴, Ye Xu², Nataliya Tsud^{1*}

- ¹ Charles University, Faculty of Mathematics and Physics, Department of Surface and Plasma Science, V Holešovičkách 2, Prague, 18000, Czech Republic
- ² Cain Department of Chemical Engineering, Louisiana State University, Baton Rouge, LA 70808, USA
- ³ Department of Biomedical and Chemical Engineering, Syracuse University, Syracuse, NY 13244, USA
- ⁴ Elettra-Sincrotrone Trieste S.C.p.A., in Area Science Park, Strada Statale 14, km 163.5, Basovizza (Trieste), 34149, Italy
- ^a Present address: FZU Institute of Physics of the Czech Academy of Sciences, Na Slovance 2, Prague, 18221, Czech Republic
- ^b Present address: Australian Synchrotron, ANSTO, 800 Blackburn Road, Clayton, VIC, 3168, Australia
- *Corresponding author: e-mail Nataliya.Tsud@mff.cuni.cz

Abstract

The adsorption of adenine on the $CeO_2(111)/Cu(111)$ surface in vacuum was studied by photoelectron spectroscopy, resonant photoelectron spectroscopy and near-edge X-ray absorption fine structure spectroscopy, and the present work describes in detail the bonding of the molecule to the ordered stoichiometric cerium dioxide film. The experimental findings were supported by density functional theory (DFT+U) analysis of different adsorption geometries of adenine on $CeO_2(111)$. The phase with adenine lying flat on the surface dominates on $CeO_2(111)$ up to 0.1 monolayer (ML) of adenine coverage. The mobility of single molecules was apparently sufficiently high to allow diffusion and formation of chain structures, which were observed to be stable in the temperature range from 25 to 250 °C. Beyond 0.1 ML, adenine molecules adsorb predominantly in an upright orientation. This phase, stable up to 120 °C, is according to theory stabilised via N3/Ce⁴⁺ and N9H/O²⁻. It was further complemented by experimental findings demonstrating the free N10H₂ group of adsorbed molecules. Thus, the saturation coverage of adenine on $CeO_2(111)$, 0.23 ML, is most likely characterised by a combination of parallel and upright bound molecules with adsorption energies of -1.01~-1.49 eV and -1.13~-1.26 eV, respectively.

1. Introduction

Purine nucleobases adsorbed on metal or oxide surface are typical model systems studied with the aim to obtain fundamental information on bonding strength and molecular adsorption geometry of the smallest building blocks of DNA on an inorganic substrate. The necessity to consider model systems comes from the complexity of real biomolecules, and fast development of biotechnology for medical diagnostics and treatments, where organic/inorganic interfaces are widely employed. [1] A recent review on electrochemical biosensing of purine nucleobases [2] emphasises the importance of basic knowledge of the molecules` interaction with the electrode surface. To improve the detection of electrochemical signals of purine nucleobases, there is a need to search for novel electrode materials.

In the present work, the stoichiometric, ordered cerium oxide film was chosen as a model substrate for adenine. Adenine is one of the building blocks of DNA and RNA and its derivatives take part in various important biological processes such as cellular respiration and protein synthesis. Cerium oxide is an inorganic material with a promising future in biosensing devices, disease diagnostics and treatments. Cerium ions can easily change their valence state between 4+ and 3+ and act either as reducing or oxidizing agents in reactions with biomolecules or living cells. The state-of-the-art regarding the physicochemical properties of nanostructured cerium oxide in bio-applications is reviewed in our recent work on adenine adsorption on nanostructured cerium oxide films. [3] Since the paper was published, the number of studies on biosensing characteristics of cerium oxide has been continuously increasing with emphasis on preparation of biocompatible nanomaterials, [4,5] their usage as a component of electrode material [6–8] or as a part of a recognition element. [9,10] Furthermore, cerium oxide nanoparticles have been shown to mimic superoxide dismutase and catalase properties. The enzymatic activity of cerium oxide was demonstrated to have therapeutic effects, reducing the oxidative stress in living cells. [11,12]

There are various reports on adenine bonding to single crystalline surfaces of noble and transition metals such as Au(111), [13] Cu(111) [14] and Cu(110) [15] (see also references cited therein). Although the recent review by S. G. Harroun [16] emphasizes the discrepancies in the reported adenine orientation on gold and silver, experimental data show a general trend — the formation of planar adsorption geometries for low adenine coverage of about 0.1 monolayer (ML) deposited in vacuum on well-ordered inorganic surfaces. In each case the question about which adenine atoms bound to a surface was resolved by density functional theory (DFT)

calculations, because the complex structure of adenine with 5 carbon and 5 nitrogen atoms $(C_5N_5H_5$, see inset of Fig. 1a) precludes the possibility of determination of the bonding structure purely experimentally.

The number of experimental and/or theoretical studies of cerium oxide model substrates for reactions with small organic and other molecules is continuously increasing. They include the interaction of SO₂, [17] methanol, [18–20] ethanol, [21] ethylene glycol, [21] formic acid, [22,23] acetic acid [21,24,25] and phosphate esters [26,27] with the oxide surface, with the aim to explore the catalytic properties of cerium oxide. The experimental works are based mainly on photoelectron spectroscopy (PES), resonant PES (RPES) [17,19–21,23,24] and infrared spectroscopy. [22] The reported DFT studies [22,26,28] commonly employ the generalised gradient approximation (GGA) and adding a Hubbard U term to the GGA exchange correlation functional to account for the strong interaction among localised 4f electrons in Ce cations in different oxidation states.

In our recent paper [3] we investigated in detail adenine bonding to cerium oxide of different stoichiometry, morphology and composition. The thermal stability of the saturated molecular adlayer prepared either in vacuum or from aqueous solution was studied in the temperature range from 25 to 250 °C. Based on the experimental data, we concluded that adenine chemisorbs on CeO₂ via nitrogen atoms, independently of the oxide morphology and deposition technique. As the experimental results were insufficient to determine the exact adsorption geometry of adenine, we tentatively suggested that the bonds were formed via N9 and N3 atoms (see inset of Fig. 1a for labelling). To test this assumption, in the present work we combined an experimental study with DFT calculations. Low coverage and saturated adlayers of adenine on the model CeO₂(111) surface obtained as a result of stepwise adenine deposition in vacuum, as well as their thermal evolution, were studied by PES, RPES, near-edge X-ray absorption fine structure spectroscopy (NEXAFS). Although the dominant tautomer of adenine is expected to be the canonical N9H form during the molecular evaporation in vacuum, DFT calculations were performed for three adenine tautomers N3H, N7H and N9H with hydrogen at the N3, N7 and N9 nitrogen atoms, respectively.

2. Experimental section

2.1. Sample preparation and experimental techniques

The experimental work was performed at Elettra-Sincrotrone Trieste (Materials Science Beamline). A detailed description of the end station can be found in Ref. [3]. The base pressure in the experimental chamber was lower than 2×10^{-10} mbar.

The CeO₂(111) film was grown in vacuum on a Cu(111) substrate (MaTecK GmbH, 99.999%). Cycles of Ar⁺ ion sputtering and annealing at 450 °C allowed us to prepare a clean Cu(111) surface before oxide deposition with negligible C 1s photoelectron signal and a sharp (1×1) low energy electron diffraction (LEED) pattern. The CeO₂(111) film was deposited by evaporation of cerium (Goodfellow, 99.99%) in an oxygen atmosphere (5×10⁻⁷ mbar) onto Cu(111) at 250 °C, followed by annealing of the film at 250 °C in O₂ at the same pressure for 10 min. The (1×1) CeO₂(111) surface structure ((1.5×1.5) with respect to that of Cu(111)) was confirmed by LEED.

A Knudsen cell evaporator, mounted in the preparation chamber with pressure of 5×10^{-9} mbar, was used for adenine (Alfa Aesar, 99%) deposition. The molecular powder was evaporated at 105 °C onto the $CeO_2(111)$ substrate at 25 °C.

For PES analysis, the core level spectra were acquired with photon energy 410 (C 1s), 475 (N 1s) and 1486.6 eV (Ce 3d, C 1s, N 1s, O 1s, Cu 2p_{3/2}) and total resolution 0.40, 0.55 and 1.0 eV, respectively. For RPES analysis the valence band (VB) spectra with total resolution of 0.16 eV were measured at 115, 121.4 and 124.8 eV photon energy. The emission from Ce 4f states located at 1.4 eV binding energy (BE) in 121.4 eV spectrum correspond to the D(Ce³⁺) resonant enhancements in Ce³⁺ cation. The signal from hybridized oxygen-cerium states at about 4.0 eV in the 124.8 eV spectrum is assigned to D(Ce⁴⁺) resonant enhancements in the Ce⁴⁺ cation. The 115 eV spectrum reports the off-resonance intensity for the D(Ce³⁺) and D(Ce⁴⁺) features (for details see S1.1. of the SI). The D(Ce³⁺)/D(Ce⁴⁺) resonant enhancement ratio (RER) was analysed. [3] The RER value for clean stoichiometric CeO₂(111)/Cu(111) surface was 0.01. The photoelectron emission angle was 0° and 20° with respect to the sample normal for synchrotron light and the X-ray source, respectively. The intensity of the photoemission peaks acquired with synchrotron light was normalized to the incident photon flux. The C 1s spectrum was stable during one acquisition step (about 30 min), and then the sample was slightly shifted to avoid radiation damage due to long illumination.

For the NEXAFS analysis, the C and N K-edges spectra were taken using the carbon and nitrogen KVV Auger yield, at normal (NI, 90°) and grazing (GI, 10°) incidence of the photon beam with respect to the surface, and with an estimated energy resolution of 0.23 and 0.38 eV,

respectively. The polarisation of light from the beamline is believed to be at least 90 % linear, as the source is a bending magnet. The corresponding background signal of the clean (i.e. C- and N-free) sample recorded under identical conditions was subtracted from the normalized raw NEXAFS spectra recorded on molecular adlayers.

The effective thickness of the oxide film and the molecular adlayers (at saturation and low adenine coverages on CeO₂(111)/Cu(111) after 75 °C annealing) was calculated from the attenuation of the Cu 2p_{3/2} core level and reported in Table 1; for details refer to Section S1.2. of the SI. We emphasise that these values provide qualitative information on the adlayer thickness obtained under the assumption of layer-by-layer growth. Thus, this approach is more suitable for the oxide film thickness calculation and less reliable for the molecular adlayer, where the adenine film is expected to partially cover the oxide surface. In this case, the adenine coverage can be expressed as the number of molecules per surface Ce cation and was estimated from the N 1s and Ce 3d core level integrated intensities ratio excited by photon energy 1486.6 eV. Coverages of 0.23 and 0.05 ML (i.e. molecule per surface Ce atom) were found for adenine adlayers at saturation and low coverages, respectively, after annealing at 75 °C, assuming all weakly bonded molecules had desorbed (see for details Table 1 and S1.3. section of the SI).

2.2.Computational methods

Periodic DFT calculations were performed in the generalized gradient approximation (GGA-PW91 [29]) and with the optB86b van der Waals (optB86b-vdW) functional [30–33] as implemented in the Vienna Ab initio Simulation Package (VASP). [34–37] Potentials due to core electrons were described using the projector-augmented wave (PAW) method, [38,39] and valence states [Ce-(5s5p4f5d6s), O(2s2p), N(2s2p), C(2s2p), H(1s)] were expanded in a plane wave basis set with a cut-off energy of 400 eV.

The thermodynamically most stable (111) facet of CeO_2 was modelled as a slab consisting of three O–Ce–O trilayers with a p(3×3) surface unit cell. Periodic slabs were separated by up to ~14 Å of vacuum, with dipole decoupling applied in the z direction. [40] A Γ -centred Monkhorst-Pack 2×2×1 k-point grid was used to sample the surface Brillouin zone. [41] The DFT+U approach of Dudarev et al. [42] was employed with a U_{eff} value of 2 eV. [22,25,26] The equilibrium lattice constant of bulk CeO_2 was calculated to be 5.476 Å (PW91) and 5.452 Å (optB86b-vdW), in close agreement with the experimental value of 5.41 Å. [43,44]

Adsorption of a single adenine molecule per p(3×3) surface unit cell corresponded to 1/9 ML coverage locally. The coordinates of the bottom two trilayers of the slab were fixed, and those of the top trilayer and adenine were fully relaxed. Geometry optimization was carried out until the maximum residual force was ≤ 0.03 eV/Å in each relaxed degree of freedom. The adsorption energy, $\Delta E_{\rm ads}$, was evaluated as $\Delta E_{\rm ads} = E_{\rm total} - E_{\rm slab} - E_{\rm gas}$, where $E_{\rm total}$, $E_{\rm slab}$, and $E_{\rm gas}$ refer to the total energies of the slab with adenine adsorbed thereon, the clean slab, and adenine in the gas phase, respectively. A more negative value of $\Delta E_{\rm ads}$ indicates stronger bonding between the adsorbate and CeO₂(111). Possible contributions from vdW interactions due to the delocalized charge densities of adenine were accounted for by re-optimizing selected GGA-PW91 adsorbed states using optB86b-vdW. Fundamental vibrational modes and frequencies were calculated to determine the zero point energies (ZPE) for selected states, evaluated as $E_{\rm ZPE} = 1/2\Sigma_i h v_i$ where v_i , are the vibrational frequencies and h is the Planck constant. A finite difference approximation approach of the dynamical matrix was used with a displacement of 0.01 Å. Very soft modes below 50 cm⁻¹ were replaced with 50 cm⁻¹ in calculating ZPEs.

The isolated gas phase N9H, N3H and N7H tautomers of adenine were optimized in an $18.0 \times 18.2 \times 18.4 \text{ Å}^3$ cubic simulation cell with dipole decoupling applied in all directions, and the reciprocal space integration at the Γ point only. Both GGA-PW91 and optB86b-vdw predicted the N9H tautomer to be more stable than the N3H and N7H tautomers by 0.29 eV and 0.33 eV, respectively, consistent with previous reports. [13,45]

3. Results

3.1. Saturated adenine adlayer on $CeO_2(111) - 0.23 ML$

After stepwise deposition, the saturated adenine adlayer defined as 0.23 ML (see above), was reached in 13 steps, corresponding to total deposition time of 540 s, on 2.3 nm thick CeO₂(111) at 25 °C. After each step the surface was analysed by PES and RPES. NEXAFS spectra were acquired only for selected coverages. The plateau in the C 1s and N 1s integrated intensity, normalized to the photoionization cross sections, [46] versus deposition time (see Fig. 1a) appeared after 300 s deposition, and was preceded by two linear segments from 0 to 150 s and 150 to 300 s. For the first deposition regime, the ratio of C 1s and N 1s intensities was almost constant with the final coverage estimated as half of saturation, i.e. about 0.10 ML. Beyond 150 s of deposition time, the C 1s signal increased systematically faster than N 1s, which can be linked with the change of the adsorption geometry of adenine. After the last deposition step, i.e. after 540 s, the ratio of N 1s to C 1s signals at 1486.6 eV photon energy, normalized to the cross

sections, [46] was 1:1.1, corresponding well to the atomic composition of adenine (see inset in Fig. 1a).

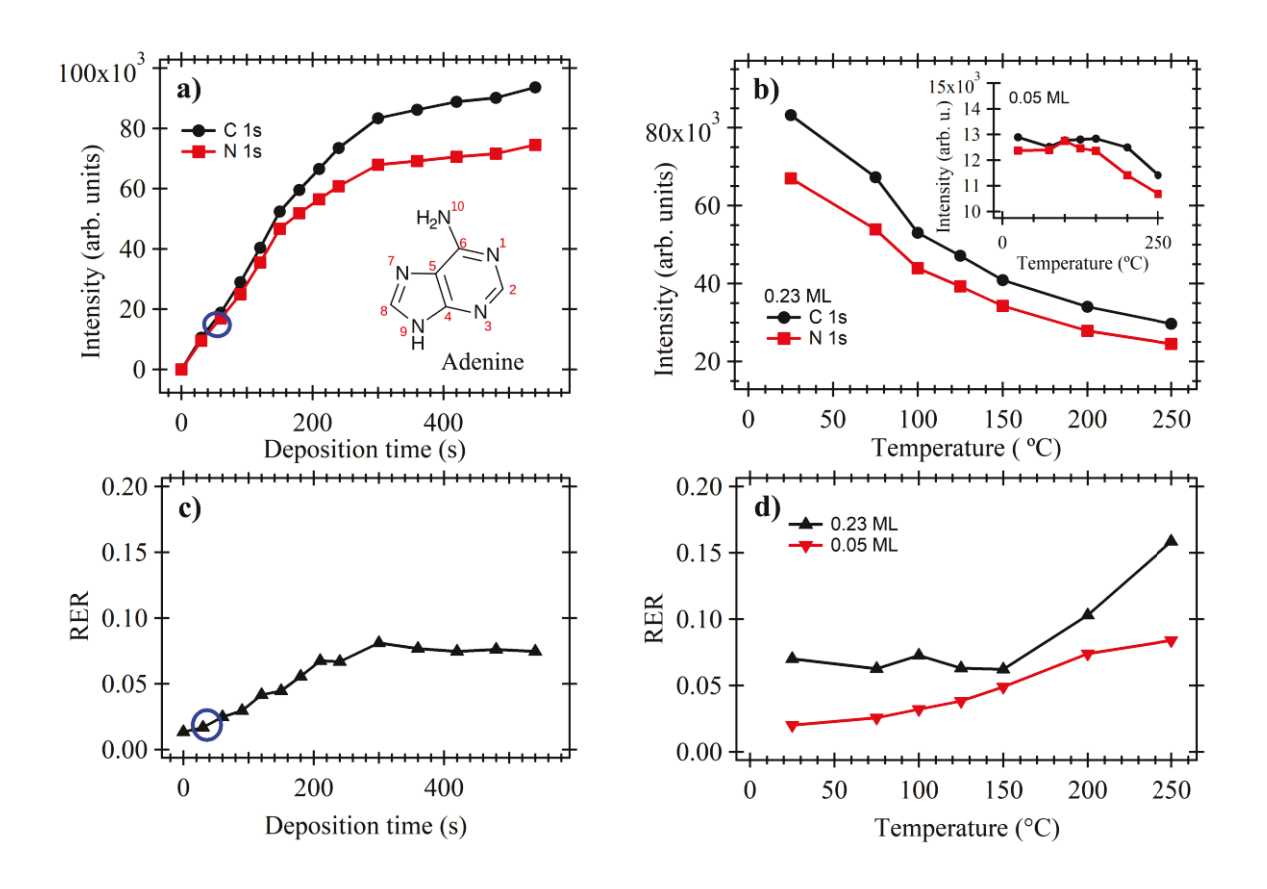


Fig. 1. The C 1s and N 1s core level intensities versus adenine deposition time for 0.23 ML (a) and versus annealing temperature for 0.23 ML and 0.05 ML (b) of adenine on $CeO_2(111)$. RER dependence on deposition time for 0.23 ML (c) and annealing temperature for 0.23 ML and 0.05 ML (d) adenine adlayers on $CeO_2(111)$. The blue circle in (a) and (c) indicates the signals that correspond to 0.05 ML adenine coverage after 75 °C. Inset in (a): the schematic structure of adenine $(C_5N_5H_5)$ and labelling of the atoms. Photon energy 410 eV for C 1s and 475 eV for N 1s core level.

The RPES results are displayed as a RER (see Experimental section) versus deposition time in Fig. 1c. We observed linearly increasing behaviour until the saturation molecular adlayer was reached, i.e. the RER of 0.01 for clean CeO₂(111) became 0.07 after 300 s deposition of adenine. The increase of the RER value indicates a weak reduction of surface Ce⁴⁺ cations during the adenine adsorption, as a result of direct interaction of molecules with the oxide surface. Once all the available adsorption sites for adenine at the interface are occupied the RER

value reaches a plateau for deposition time at 300 to 540 s. The surface reduction of the cerium oxide film mostly has an electronic character, as there was no change in the O 1s core level (spectra not shown). The charge transfer from adenine to the surface Ce^{4+} cations for a saturation adlayer on $CeO_2(111)$ was tentatively estimated (for details, see S2. of the SI) to be $0.04~e^-$ per adenine molecule.

Table 1. Thickness of the $CeO_2(111)$ film (d_{ox}, nm) ; effective thickness of adenine adlayers (d_{ade}, nm) ; ratio of N 1s signal to estimated surface contribution of Ce 3d signal of clean $CeO_2(111)$, $I_{tot}(N 1s) / I_{surf}(Ce 3d)_{before}$; adenine coverage (ML) for molecular adlayers on $CeO_2(111)$ after treatment at 75 °C.

1486.6 eV	Adenine/CeO ₂ (111)	Adenine/CeO ₂ (111)	
photon energy	540 sec, 75 °C	30 sec, 75 °C	
d _{ox} , nm	2.3	2.0	
d _{ade} , nm	0.44	0.13	
Itot(N 1s)/ Isurf(Ce 3d)before	1.10	0.21	
coverage, ML	0.23	0.05	

The evolution of the N 1s and C 1s core level spectra of adenine/CeO₂(111) system during the stepwise molecular deposition is shown in Fig. 2. The N 1s signal is dominated by component B at BE of 399.0 eV in the first deposition regime, i.e. until 150 s. A second component A develops on the high BE side, at 400.6 eV, starting from 150 s deposition time. Following the literature, [3,15] the components are assigned as follows. The imino nitrogen atoms N1, N3 and N7 contribute mainly to peak B and amino N9 and N10 atoms to peak A. The absence of component A in the first deposition regime indicates a change of the electronic configuration of the amino nitrogen atoms of adenine. Here we expect either bonding of the molecule via an amino nitrogen atom to the surface, or stabilization of the molecular arrangement on the surface via hydrogen bond networks involving amino nitrogen atoms. The A to B intensity ratio for the saturated adenine adlayer on CeO₂(111), for instance that which corresponds to 480 s of deposition time, is 1:3.4, far from the expected nominal 1:1.5 ratio for adenine. This implies that the molecular adsorption geometry for the saturated adlayer has mixed character, i.e. either the first phase up to 150 s, characterized by a single component B, is complemented by adenine molecules that were bonded differently (from 150 s to 300 s deposition time) or a gradual phase transition occurs, which affects all adsorbed species. The shape of the C 1s spectrum compared

to N 1s is more complex, so a straightforward component identification is complicated. For the 480 s deposition, we tentatively fit the C 1s spectrum in two components C and D at BEs of 286.8 eV and 285.6 eV, respectively. Moreover, the two-component structure of the C 1s core level is present even for the first deposition regime, for instance see the 60 s deposition spectrum. According to the literature [3,15] the C2, C4, C6 and C8 adenine atoms contribute to component C, and C5 to component D. The ratio of the components is not further analysed here because of the uncertainties of the proposed fit, as the ratio value is mainly defined by the reliability of the fitting procedure applied to the spectral line. Obviously, we have a different component distribution due to the complex geometry of the adsorbed adenine molecule.

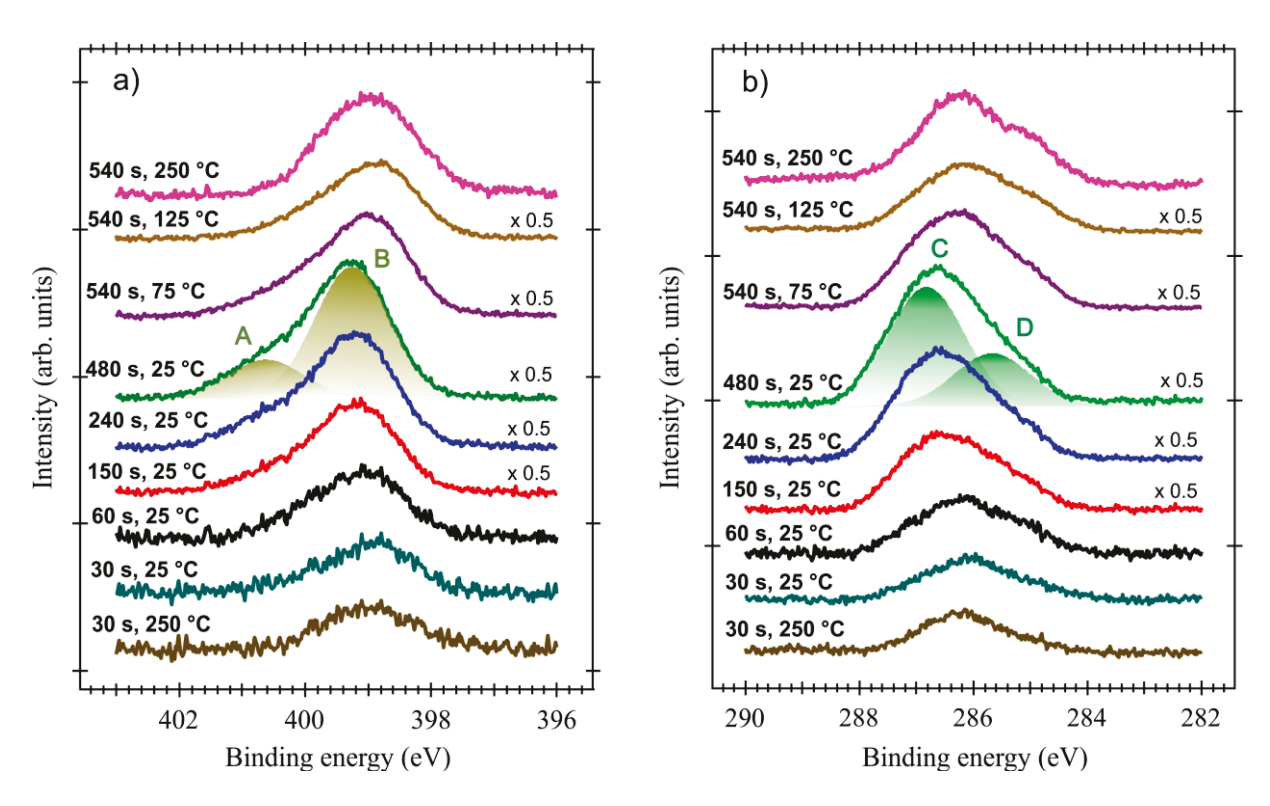


Fig. 2. N 1s (a) and C 1s (b) core level spectra of adenine on CeO₂(111) after the indicated deposition times and thermal treatment. Photon energy 475 eV for N 1s and 410 eV for C 1s spectra.

The N K-edge NEXAFS spectra for selected adenine adlayers are shown in Fig. 3 measured at GI and NI. The observed spectral shape is typical for adenine. [3,47,48] The sharp peak at 400.0 eV is due to a π^* resonance, i.e. excitation of N 1s electrons to the lowest unoccupied molecular orbitals of π^* symmetry, and the broad features at 407.0 eV and 412.0 eV originate from excitation of electrons to σ^* orbitals. The ratio of π^* to σ^* intensities is shown in the Table 2.

All amino and imino nitrogen atoms of the purine ring contribute to the aforementioned π^* and σ^* resonance features, and it is not possible to distinguish individual single electron excitations. [48] However, useful structural information was extracted from the comparison of the NEXAFS spectra acquired at the two geometries GI and NI. For the first deposition regime of adenine (30 sec spectrum) a clear angular dependence was observed in the NEXAFS spectra. The π^* relative to the σ^* resonance peak has maximum intensity at GI (2.39, see Table 2) and minimum intensity at NI (0.63). Thus the molecules are absorbed on the oxide surface with the rings parallel to the surface since when the incident photon beam is mostly linearly polarised and at GI geometry, the π^* orbitals perpendicular to the surface are predominantly excited. As the deposition time increases, the π^* resonance peak in NI spectra grows and the difference between the GI and NI spectra becomes less pronounced. We were not able to detect a preferential molecular adsorption orientation for the saturation adenine adlayer. The C K-edge NEXAFS spectra (data not shown here) had a single π^* resonance component as in Ref. [3] for adenine/CeO2. The π^* to σ^* intensity ratio values were similar to the N K-edge data confirming the conclusions on adsorption geometry.

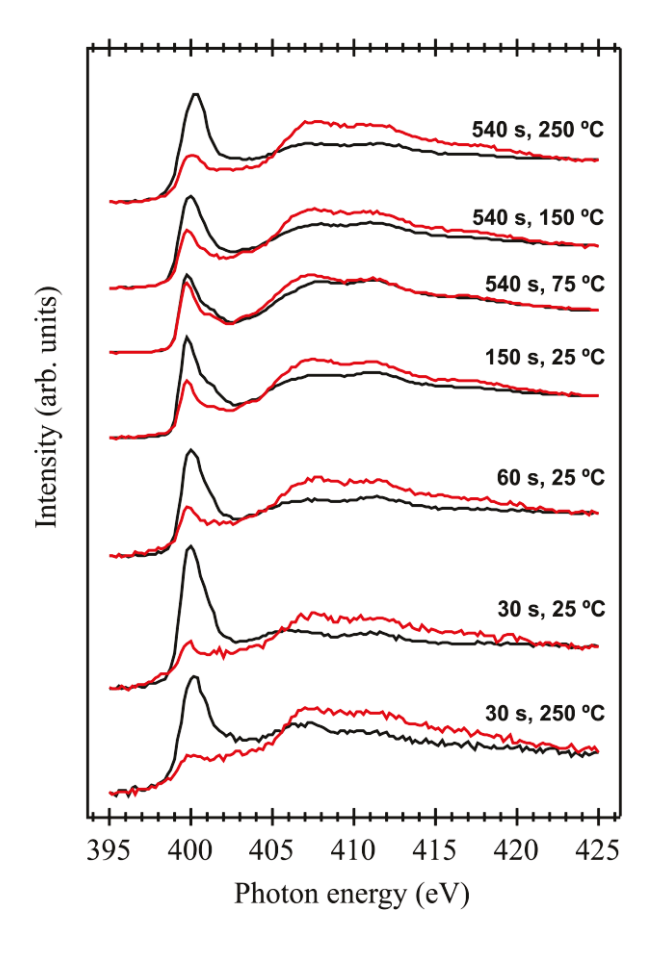


Fig. 3. N K-edge NEXAFS spectra of adenine on CeO₂(111) surface after the indicated deposition times and thermal treatment, measured in two geometries: GI (black line) and NI (red line).

Table 2. The N K-edge spectral characteristics: ratio of maximum intensities of the π^* to σ^* resonances for spectra taken at different geometries, and the excitation energy (eV) of the π^* peak.

Sample	N K-edge, GI (NI)	Excitation energy, π^* (eV)	
30 s, 25 °C	2.39 (0.63)	400.0	
30 s, 250 °C	1.64 (0.46)	400.2	
60 s, 25 °C	1.86 (0.63)	400.0	
150 s, 25 °C	1.60 (0.72)	399.8	
540 s, 75 °C	1.09 (0.90)	399.8	
540 s, 150 °C	1.43 (0.73)	400.0	
540 s, 250 °C	1.81 (0.59)	400.3	

3.2. Thermal treatment of saturated and low-coverage adenine adlayers on $CeO_2(111)$ – 0.23 ML, 0.05 ML

The thermal evolution of adenine adlayers on CeO₂(111) was studied by annealing them in vacuum for 1 min at 75, 100, 125, 150, 200 and 250 °C. The thermal treatment of the saturation adenine adlayer on CeO₂(111) (0.23 ML) induces molecular desorption of the weakly bound species, leading to a decrease of the C 1s and N 1s integrated intensity (Fig. 1b). The RER is stable up to 150 °C and then increases from 0.07 to 0.16 after 250 °C (Fig. 1d). Up to 200 °C, the shapes of the N 1s and C 1s spectra are mostly conserved while the peak maxima shift to lower BE by about 0.4 eV (Fig. 2). Annealing at 250 °C causes a little change of the shape of both core level spectra, indicating variations in the local electronic structure of the carbon and nitrogen atoms of the adsorbate.

The thermal treatment causes changes in the NEXAFS spectra of the 0.23 ML adenine/CeO₂ layer in the reverse order with respect to that observed during stepwise deposition, consistent with the molecular desorption seen in the PES data. It may indicate that the flat-lying adenine phase is the most stable, and these molecules are decorated by adsorbed species in another

geometry when the coverage increases. The change of the π^* resonance peak energy is consistent with the shifts of the N 1s and C 1s photoemission peaks. The shape of the π^* resonance peak is slightly different after the final annealing at 250 °C, again supporting the idea of the electronic structure adjustment of nitrogen and carbon atoms of adsorbed adenine seen in the N 1s and C 1s spectra (Fig. 2).

The first deposition step of adenine on CeO₂(111) was repeated and defined as low coverage, i.e. 0.05 ML, the thermal stability of which was checked in the same way as for the saturated adlayer (0.23 ML). It was observed that the molecular adlayer was stable at all annealing steps. For this reason, the N 1s (Fig. 2a), C 1s (Fig. 2b) and N K-edge (Fig. 3) spectral characteristic lines are reported only for as-deposited adlayer and after the final annealing at 250 °C. In Fig. 1a,c the 0.05 ML adenine/CeO₂(111) surface after treatment at 75 °C is represented by blue circles, which fall into the first deposition regime. The C 1s and N 1s intensity behaviour versus temperature is shown in the inset of Fig. 1b. Both signals are almost stable up to 150 °C, and then they start to decrease, reaching an only slightly lower coverage of 0.04 ML after heating to 250 °C. The RER value increases with temperature, but the absolute value remains lower than that one for 0.23 ML (see Fig. 1d).

3.3. DFT calculations for adenine on $CeO_2(111)$

The adsorption of isolated N9H, N3H and N7H tautomers of adenine on $CeO_2(111)$ was modelled and calculated using DFT. Adenine can potentially interact with a Ce^{4+} site via a nitrogen atom, with an O^{2-} site via an acidic hydrogen atom in an amino group, or with both simultaneously. The orientations that we investigated were chosen so that such interactions were favoured. The energy-minimized states had the molecular plane of adenine in a variety of positions with respect to the surface, which we characterize with the angle (α) between the surface normal and the purine rings to give a measure of how tilted away from the surface normal the molecule is. Here, those states with $\alpha > 60^{\circ}$ are referred to as parallel states, and those with $\alpha < 60^{\circ}$ as upright states, although the distinction is somewhat arbitrary. The more stable states and the corresponding adsorption energies (ΔE_{ads}) are reported in Table 3.

Table 3. Minimum-energy adsorption states and energies (ΔE_{ads} , in eV per molecule) calculated using GGA-PW91 and optB86b-vdW for the N9H, N3H, and N7H tautomers of adenine in various degrees of tilt with respect to the surface normal (α , in °).

Adsorption	Interaction	α (°)	$\Delta E_{ m ads}$	$\Delta E_{ m ads}$
states (figure)			GGA-PW91	optB86b-vdW
N9H parallel				
(Fig. 4a)	N10/Ce ⁴⁺	67	-0.29	-1.01
(Fig. 4b)	N10/Ce ⁴⁺ (N9H, N10H dissociated)	75	+0.74	
	N9/Ce ⁴⁺	75	-0.26	
(Fig. 4c)	H-bonded chain †	83, 85	-0.58	-1.49
N9H upright				
(Fig. 4d)	N3/Ce ⁴⁺ , N9H/O ²⁻	29	-0.58	-1.13
	N3/Ce ⁴⁺ , N9H/O ^{2- †}	28, 29	-0.65	-1.26
(Fig. 4e)	N3/Ce ⁴⁺ , N9/HO (N9H dissociated)	29	-0.37	
	N1/Ce ⁴⁺ , N10H/O ²⁻	23	-0.43	
	N7/Ce ⁴⁺ , N10H/O ²⁻	22	-0.13	
	C2H/O ²⁻	10	-0.27	
N3H parallel				
(Fig. 4f)	N10/Ce ⁴⁺	67	-0.30	-1.00
	$N3/Ce^{4+}$	77	-0.21	
N3H upright				
(Fig. 4g)	N3H/O ²⁻ , N9/Ce ⁴⁺	13	-0.83	-1.32
	N1/Ce ⁴⁺ , N10H/O ²⁻	23	-0.39	
	N7/Ce ⁴⁺ , N10H/O ²⁻	23	-0.13	
N7H parallel				
(Fig. 4h)	N10/Ce ⁴⁺	67	-0.40	-1.14
	N7/Ce ⁴⁺	85	-0.15	
N7H upright				
(Fig. 4i)	N1/Ce ⁴⁺ , N10H/O ²⁻	23	-0.50	-1.04
	N7H/O ²⁻ , N10H/O ²⁻	58	-0.49	
	N3/Ce ⁴⁺ , N9/Ce ⁴⁺	38	-0.32	

Coverage is 1/9 ML except where noted. α is based on GGA-PW91 geometries.

[†] With two adenine molecules per p(3×3) unit cell, equivalent to 2/9 ML locally. ΔE_{ads} is the average of the two molecules.

[&]quot;X/Y" in the "Interaction" column indicates an atom X in adenine is located on a site Y in $CeO_2(111)$. Selected states that are depicted in Fig. 4 are indicated.

The more stable parallel states involve the N10 atom located over a Ce^{4+} site. This is because, besides $N^{\delta-}$ - Ce^{4+} interaction, the N10H₂ group can coordinate to one or two adjacent O^{2-} sites via the acidic H atoms. Thus adenine is not completely flat in the most stable parallel states, with N10 being closest to the surface and the rest of the molecule tilted further away from the surface (Fig. 4a, 4f, and 4h).

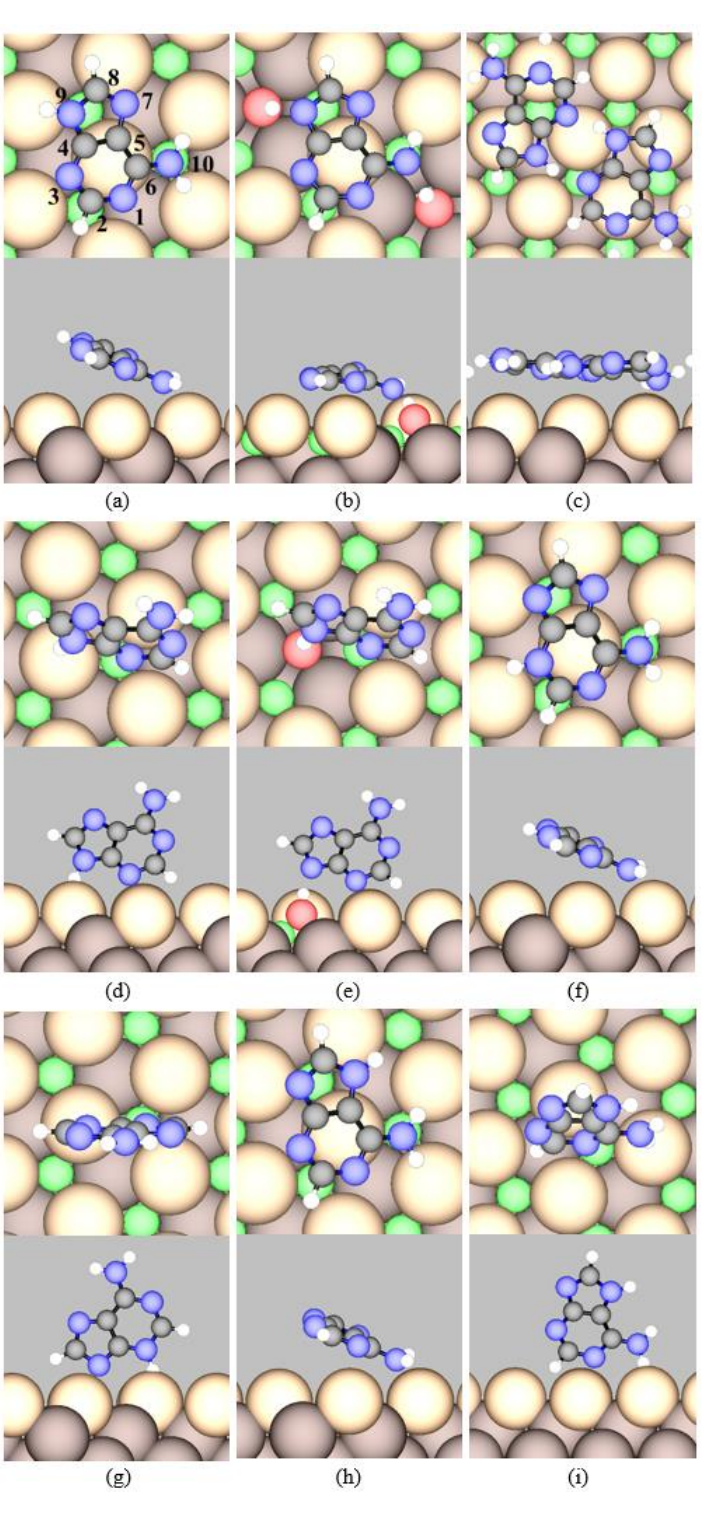


Fig. 4. Top and side views (top and bottom panels, respectively) of selected GGA-PW91 energy-minimized structures of adenine adsorbed on a p(3×3) surface unit cell: For N9H tautomer, a) parallel – N10/Ce⁴⁺, b) parallel – N10/Ce⁴⁺ (N9H, N10H dissociated), c) parallel – H-bonded chain, d) upright – N3/Ce⁴⁺, N9H/O²⁻, e) upright – N3/Ce⁴⁺, N9H/O²⁻ (N9H dissociated); for N3H tautomer, f) parallel – N10/Ce⁴⁺, g) upright – N3H/O²⁻, N9/Ce⁴⁺; for N7H tautomer, h) parallel – N10/Ce⁴⁺, and i) upright – N1/Ce⁴⁺, N10H/O²⁻. Colour code: green=Ce⁴⁺, light brown=surface O²⁻, dark brown=subsurface O²⁻, red=surface O²⁻ with H adsorbed on it, black=C, blue=N, and white=H. Images are created using VESTA. [49] Numbering of the backbone atoms in (a) is the same as in the inset in Fig. 1a.

Adjacent adenine molecules adsorbed in parallel orientations may form hydrogen bonds between N atoms and acidic H atoms in the amino groups. The formation of hydrogen-bonded networks has previously been reported in STM studies for adenine deposited on Au(111) at temperatures 100–170 K, [50–52] which was corroborated by DFT calculations. [13] We considered this possibility by constructing a model hydrogen-bonded chain structure of adenine consisting of two N9H tautomers per p(3×3) surface unit cell adsorbed in parallel orientations (Fig. 4c). Significant stabilization (by 0.48 eV in optB86b-vdW) was predicted compared to an isolated N9H tautomer in the most stable parallel state, which is approximately the strengths of four hydrogen bonds of the N–H–N type.

Isolated adenine adsorbed in upright states is generally more stable than in parallel states because the upright orientation permits multiple points of interaction between adenine and the surface. It should be noted that the molecular plane of adenine tends to be slightly tilted with respect to the surface normal. The more favourable configurations involve a nitrogen atom located above a Ce^{4+} site and an N–H atom located above an O^{2-} site ((N/Ce⁴⁺, NH/O²⁻) states). The N9H and N3H tautomers have (N3, N9H) and (N9, N3H) centres, respectively, in close proximity to engage in such interaction while bringing the molecule close to the surface (Fig. 4d and 4g). These turn out to be the most favourable upright adsorption configurations. Alternative configurations involving adenine interacting with the surface through N10H and either N1 or N7 are somewhat less stable. In addition to the (N/Ce⁴⁺, NH/O²⁻) states, adenine states interacting with the surface through (N/Ce⁴⁺, N/Ce⁴⁺) or through (CH/O²⁻) were also considered but were never found to be the most stable states for a given tautomer. Upon inclusion of vdW interactions, the ΔE_{ads} of the most stable parallel and upright states for an

isolated adenine molecule become more exothermic by ca. 0.7 and 0.5 eV, respectively, which reduces the difference in stability between parallel and upright states somewhat.

As the CeO₂(111) film in this study was grown under oxidizing conditions, we expect oxygen vacancies to play a negligible role in molecular adsorption of adenine. If any oxygen vacancies existed, they would likely have occupied subsurface sites. [53] We have therefore also examined the effect of an oxygen vacancy in the immediate subsurface (i.e., on the bottom O layer of the top O-Ce-O trilayer, denoted V_O^{SS}) on the adsorption of the N9H tautomer as an example. When a V_O^{SS} is located at various positions directly beneath the most stable upright state (N3/Ce⁴⁺, N9H/O²⁻) or the parallel H-bonded chain state, ΔE_{ads} was found to vary by less than ± 0.1 eV in each case. The effect of a surface oxygen vacancy on adenine adsorption, as may occur on a partially reduced ceria film, will be the subject of a future study.

Given the amphoteric nature of the $CeO_2(111)$ surface, we further considered for the N9H tautomer the deprotonation of the amino group (N9H) in an upright state, and the deprotonation of both amino groups (N9H and N10H₂), which yields a closed-shell species, in a parallel state. The dissociated H atom(s) was adsorbed on a nearest O^{2-} site and remained hydrogen-bonded to the N centres from which they originated (Fig. 4b and 4e). As can be seen in Table 3, the deprotonation of adenine by $CeO_2(111)$ is energetically unfavourable.

4. Discussion

Overall the DFT results suggest that i) the N3, N9 and N10 atoms are most significantly involved in the adsorption of isolated adenine molecules on $CeO_2(111)$; ii) hydrogen-bonded networks of adenine should be the most stable adsorption structure when the molecules are free to diffuse and assemble into such structures; and iii) isolated adenine molecules prefer upright over parallel states. These findings are consistent with the experimental observation that the parallel adsorption geometry of presumably hydrogen-bonded adenine molecules dominates up to 0.1 ML coverage, for which the N 1s signal is formed mainly by the component B (Fig. 2a) and the intensity of π^* resonances is higher at GI geometry (Fig. 3, Table 2). The appearance of the component A in the N 1s core level spectra above 150 s deposition time (Fig. 2a) corresponds to unperturbed amino N9 or N10 atoms in the adenine molecule. This could be due to additional adenine molecules adsorbed in upright geometry decorating hydrogen-bonded chains, in which they interact with the surface primarily via N9H and N3, leaving the N10H₂ amino group and two other imino nitrogen atoms unperturbed, and without clear molecular

orientation according to the NEXAFS data. Apparently at the saturation coverage 0.23 ML of adenine on CeO₂(111), a mixture of two molecular adsorption geometries coexisted with calculated maximum adsorption energies -1.49 eV for chains and -1.26 eV for the upright molecules.

For the N9H tautomer, the lowest $\Delta E_{\rm ads}$ of isolated adenine on CeO₂(111), according to the optB86b-vdW calculations, are -1.01 and -1.13 eV (Fig. 4a and 4d) in parallel and upright states, respectively, with the corresponding ZPE-corrected $\Delta E_{\rm ads}$ being -0.97 and -1.11 eV. The peak desorption temperature corresponding to such $\Delta E_{\rm ads}$ is calculated to be 100-152 °C based on the Redhead analysis [54] with 1/9 ML initial coverage, a heating rate of 10 °C s⁻¹, a desorption prefactor of 10^{13} s⁻¹, and with desorption assumed to be of first order. Likewise, based on ZPE-corrected $\Delta E_{\rm ads}$ the hydrogen-bonded chain structure (Fig. 4c) is expected to persist on CeO₂(111) to 278 °C on average, which is consistent with the experimental observation that the adenine adlayer is stable up to 250 °C. In a mixed saturation layer, individual adenine molecules adsorbed in upright orientations in the midst of hydrogen-bonded networks are expected to be appreciably less stable, and would therefore desorb at lower temperature, which is consistent with the vanishing of component A of the N 1s core level upon heating to 75 °C and higher temperature (Fig. 2a).

According to Fig 1c, the mixed phase of adsorbed molecules on CeO₂(111) is characterised by the linear increase of RER until the saturation coverage is reached. Thus we conclude that the cerium cation reduction is independent of the molecular adsorption geometry. For the low coverage adenine adlayer (0.05 ML) cerium reduction increases continuously with temperature, which was explained by the charge transfer from molecules to the oxide. It was estimated to be 0.2 e⁻ per adenine molecule after 250 °C (see S2 section of the SI). Thus the thermally induced charge transfer for the oriented 0.05 ML phase indicates that the interaction of the molecule with the oxide is weak at 25 °C and stimulated by annealing with no evident change of parallel adsorption geometry. For the saturation coverage, the molecular coverages decrease from 0.23 to 0.10 ML after 250 °C treatment. In general, the lower RER values for the 0.05 ML system compared to 0.23 ML were linked to lower molecular concentration and consequently lower charge exchange. The ordered phase of adenine on CeO₂(111) was reached for both 0.05 ML and 0.23 ML systems after 250 °C, where the RER values (0.08 and 0.16) are roughly proportional to the adenine coverage (0.04 and 0.10).

To corroborate the RER results we have performed a Bader charge analysis [55] to compare the charge state of Ce atoms in the top trilayer for the more stable N9H states (Figs 4a, 4c, and 4d) with that in the clean slab. There is no significant increase in either the total charge or the f electron population of the Ce cations, indicating that surface reduction upon molecular adsorption of adenine is unlikely. Using the H-bonded chain (Fig. 4c) as example, we observe only a minimal amount of charge density redistribution in and around the adenine (Fig. 5). Comparatively, the change in charge density is most significant at the amino N10H₂ group that is located directly above the Ce⁴⁺ site. Here there is greater charge accumulation (red contours) between the N and the surface Ce⁴⁺ site than elsewhere, and there is evidence of charge transfer from one of the acidic H atoms to the O^{2-} site beneath it. Overall these results are in line with the small variation in RER observed with respect to the clean oxide surface (0.01 to 0.07) for samples annealed at temperatures < 150 °C (Figs. 1c and 1d). A steep increase in RER to 0.16 for the saturated samples annealed beyond 150 °C could be due to formation of surface defects and water desorption.

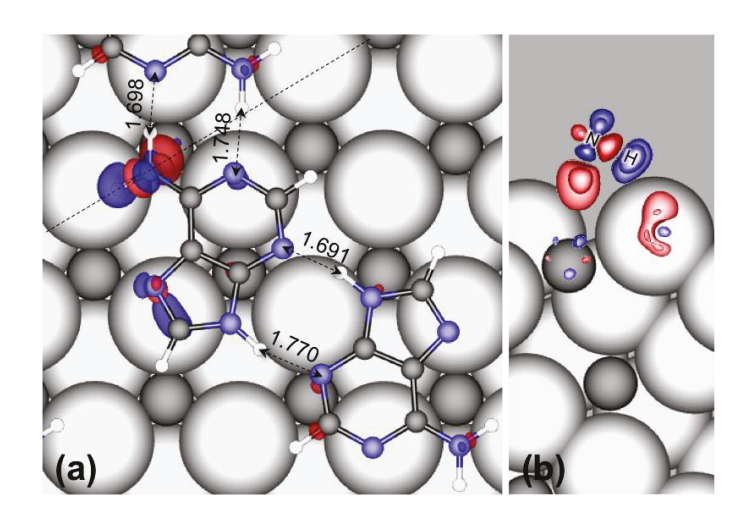


Fig. 5. (a) Top view and (b) cut-out side view of charge density difference for the H-bonded chain state ($\Delta \rho = \rho_{\text{total}} - \rho_{\text{surface}} - \rho_{\text{adenine}}$) calculated by GGA-PW91. Red and blue contours represent regimes of charge accumulation and depletion, respectively. The contour values are ± 0.001 e/ų in (a), and ± 0.001 and ± 0.002 e/ų in (b). The side view in (b) is cut out along the dashed line indicated in (a) that runs through one of the N10–H bonds, with the adenine molecules removed for clarity. The lengths of four hydrogen bonds (in Å) are indicated in (a). Colour code: black=C, blue=N, and white=H. Surface O²- and Ce⁴+ are represented by large and small grey spheres, respectively, for clarity.

Comparison of two different ways of saturated adlayer preparation, i.e. stepwise (in this work) and deposition of multilayer coverage with the subsequent thermally induced desorption of weakly bonded species (see Ref [3]) leads to the conclusion that independently of the approach, an adenine film without clear molecular surface orientation is formed. We reached a RER value of 0.16 after 250 °C annealing of 0.23 ML adenine adlayer on CeO₂(111), which is very similar to the value of 0.20 reported in Ref. [3] for the multilayer adenine/CeO₂(111) after the same treatment. Thus, the charge transfer from adenine molecules to Ce⁴⁺ ions, observed as increasing RER, for the adlayers prepared in two different ways, is comparable. We have also shown that the oriented adenine adlayer on the CeO₂(111) surface can be achieved at molecular coverage of 0.10 ML and lower.

Adenine on Au(111) [13] is a closely related system to the present study. The hydrogen-bonded parallel chains of adenine molecules on Au(111) observed by STM at low temperatures [50– 52] are characterised by a higher adsorption energy (-1.66 eV) than the value for the isolated molecule (-1.17 eV) on the same surface according to DFT, [13] similar to adenine on CeO₂(111). We conjecture that the main difference in the two systems is in the stability of hydrogen-bonded parallel chains at room temperature and/or after annealing at higher temperatures. Chain structures are not stable on Au(111) where, on average, molecules can be considered isolated. There is no published STM study confirming adenine chain formation on CeO₂(111), so we assume that the chain stability is connected with high surface reactivity of cerium oxide. Adenine on Cu(111) is another example where the ordered sub-monolayer phase of adenine was prepared by thermal treatment of the multilayer as well as sub-monolayer adenine films. The strong interaction of adenine with Cu(111) keeps the adsorbed adlayer intact within an intermolecular hydrogen bond network up to 200 °C, in agreement with our results for adenine on CeO₂(111). A transition from the flat-lying to upright adsorption geometry with increasing molecular coverage was also observed for the terephthalic acid/TiO₂(110) model system. [56] Independent of the different chemical structure of terephthalic acid compare to adenine, we suggest that the molecule-substrate interaction is mainly responsible for the specific coverage dependent molecular adlayer configurations on the corresponding oxide surface.

An alternative explanation of the strongly bound phase formation of the adsorbed molecules on $CeO_2(111)$ might be a partial deamination. Undoubtedly some of the adenine molecules simply desorb upon heating (decreasing both C and N 1s intensities), but some may undergo a reaction

at elevated temperatures (lower N 1s intensity compared to C 1s after annealing above 150 °C of 0.23 and 0.05 ML adenine). There are tentative signs that are consistent with a possibility that ceria deaminates adenine above 150 °C, forming NH₂ which might react with the acidic H to form NH₃. Ammonia would desorb readily in UHV because its adsorption energy on CeO₂(111) is weak (about -0.5 eV), leaving behind a moiety on the surface that contains 4 imino nitrogen atoms, which is consistent with one component N 1s core level spectra after 150 °C. The double ring moiety may capture an oxygen atom from the oxide lattice forming a C=O bond that can be viewed as 6-oxopurine in an oxygen vacancy and contribute to the surface oxide reduction, i.e. increasing the RER value. The adsorption energy of this molecule is close to -4 eV and explains the adlayer stability at 250 °C. Experimental data do not provide any evidence of the C=O bonding, neither in C 1s core level nor in C K edge spectra, which would support the idea of deamination. Thus further investigation should be carried out to test this hypothesis.

5. Conclusions

The adsorption geometry and thermal stability of low coverage (0.05 ML) and saturated adlayers (0.23 ML) of adenine on the CeO₂(111) surface in vacuum were studied by PES, RPES, NEXAFS spectroscopies and DFT calculations. The bonding of adenine in two distinct phases which form the saturation molecular adlayer on CeO₂(111) was defined in detail by the combination of the experimental and theoretical approaches. First, in the coverage range 0–0.1 ML, the molecules mostly adsorb with purine rings parallel to the surface. The adenine molecules apparently rearrange on the surface in hydrogen bonded chains due to their high mobility at 25 °C. The desorption temperature of this phase is higher than 250 °C with the major contribution to bonding in the interface coming from the N10H₂ amino group attracted by Ce⁴⁺ cations. Later, starting from 0.10 ML coverage, the second phase is detected with adenine molecules bonded via N3 and N9H atoms to the oxide surface with an angle of about 29° between the purine rings and the surface normal. The upright adsorbed molecules are less stable with desorption temperature of about 120 °C. The present work is in line with adenine/Au(111) and adenine/Cu(111) studies where the molecules in hydrogen-bonded network phases were detected with adsorption energies proportional to the substrate reactivity, i.e. lower for Au(111) and higher for Cu(111), with desorption temperature 120 and 200 °C, respectively. We believe that the stable hydrogen-bonded chains of the intact adenine molecules on the surface of CeO₂(111) are a promising system for further applications in (bio)organic/inorganic hybrid systems for nanotechnology.

Acknowledgements

We gratefully acknowledge the assistance of our colleagues at Elettra for providing high quality synchrotron light. CERIC-ERIC consortium and Czech Ministry of Education (LM2018116) are acknowledged for financial support. Work at Louisiana State University was supported by the U.S. National Science Foundation under Grant CHE-1664984, and used high-performance computational resources provided by LSU (https://hpc.lsu.edu), by the Center for Nanophase Materials Sciences, which is a US-DOE Office of Science User Facility, and by the National Energy Research Scientific Computing Center, which is supported by the Office of Science of US-DOE under Contract DE-AC02-05CH11231. X. H. Z. was supported through a U.S. National Science Foundation Research Experience for Undergraduates Grant (EEC-1560305) at LSU.

References

- [1] D. Costa, C.-M. Pradier, F. Tielens, L. Savio, Adsorption and self-assembly of bioorganic molecules at model surfaces: A route towards increased complexity, Surf. Sci. Rep. 70 (2015) 449–553. doi:http://dx.doi.org/10.1016/j.surfrep.2015.10.002.
- [2] V.K. Sharma, F. Jelen, L. Trnkova, Functionalized solid electrodes for electrochemical biosensing of purine nucleobases and their analogues: A review, Sensors (Switzerland). 15 (2015) 1564–1600. doi:10.3390/s150101564.
- [3] S. Bercha, K. Beranová, R.G. Acres, M. Vorokhta, M. Dubau, I. Matolínová, T. Skála, K.C. Prince, V. Matolín, N. Tsud, Thermally Controlled Bonding of Adenine to Cerium Oxide: Effect of Substrate Stoichiometry, Morphology, Composition, and Molecular Deposition Technique, J. Phys. Chem. C. 121 (2017) 25118–25131. doi:10.1021/acs.jpcc.7b06925.
- [4] F. Charbgoo, M. Ramezani, M. Darroudi, Bio-sensing applications of cerium oxide nanoparticles: Advantages and disadvantages, Biosens. Bioelectron. 96 (2017) 33–43. doi:https://doi.org/10.1016/j.bios.2017.04.037.
- [5] F. Charbgoo, M. Bin Ahmad, M. Darroudi, Cerium oxide nanoparticles: green synthesis and biological applications, Int. J. Nanomedicine. 12 (2017) 1401–1413. doi:10.2147/IJN.S124855.
- [6] C.S. Pundir, V. Narwal, Biosensing methods for determination of triglycerides: A review, Biosens. Bioelectron. 100 (2018) 214–227. doi:https://doi.org/10.1016/j.bios.2017.09.008.
- [7] N.T. Nguyet, L.T. Hai Yen, V. Van Thu, H. Lan, T. Trung, P.H. Vuong, P.D. Tam, Highly sensitive DNA sensors based on cerium oxide nanorods, J. Phys. Chem. Solids. 115 (2018) 18–25. doi:https://doi.org/10.1016/j.jpcs.2017.11.023.
- [8] Y. Kosto, A. Zanut, S. Franchi, Y. Yakovlev, I. Khalakhan, V. Matolín, K.C. Prince, G. Valenti, F. Paolucci, N. Tsud, Electrochemical activity of the polycrystalline cerium oxide films for hydrogen peroxide detection, Appl. Surf. Sci. 488 (2019) 351–359. doi:https://doi.org/10.1016/j.apsusc.2019.05.205.

- [9] G. Maduraiveeran, M. Sasidharan, V. Ganesan, Electrochemical sensor and biosensor platforms based on advanced nanomaterials for biological and biomedical applications, Biosens. Bioelectron. 103 (2018) 113–129. doi:https://doi.org/10.1016/j.bios.2017.12.031.
- [10] X. Sun, H. Wang, Y. Jian, F. Lan, L. Zhang, H. Liu, S. Ge, J. Yu, Ultrasensitive microfluidic paper-based electrochemical/visual biosensor based on spherical-like cerium dioxide catalyst for miR-21 detection, Biosens. Bioelectron. 105 (2018) 218– 225. doi:https://doi.org/10.1016/j.bios.2018.01.025.
- [11] A.R. Gliga, K. Edoff, F. Caputo, T. Källman, H. Blom, H.L. Karlsson, L. Ghibelli, E. Traversa, S. Ceccatelli, B. Fadeel, Cerium oxide nanoparticles inhibit differentiation of neural stem cells, Sci. Rep. 7 (2017) 9284. doi:10.1038/s41598-017-09430-8.
- [12] D.P. Cormode, L. Gao, H. Koo, Emerging Biomedical Applications of Enzyme-Like Catalytic Nanomaterials, Trends Biotechnol. 36 (2018) 15–29. doi:https://doi.org/10.1016/j.tibtech.2017.09.006.
- [13] R.G. Acres, X. Cheng, K. Beranová, S. Bercha, T. Skála, V. Matolín, Y. Xu, K.C. Prince, N. Tsud, An experimental and theoretical study of adenine adsorption on Au(111), Phys. Chem. Chem. Phys. 20 (2018) 4688–4698. doi:10.1039/c7cp08102b.
- [14] N. Tsud, S. Bercha, K. Ševčíková, R.G. Acres, K.C. Prince, V. Matolín, Adenine adlayers on Cu(111): XPS and NEXAFS study, J. Chem. Phys. 143 (2015) 174704– 174712. doi:10.1063/1.4935055.
- [15] V. Feyer, O. Plekan, K. Prince, F. Šutara, T. Skála, V. Cháb, V. Matolín, G. Stenuit, P. Umari, Bonding at the organic/metal interface: Adenine to Cu(110), Phys. Rev. B. 79 (2009) 155432–155437. doi:10.1103/PhysRevB.79.155432.
- [16] S.G. Harroun, The Controversial Orientation of Adenine on Gold and Silver, ChemPhysChem. 19 (2018) 1003–1015. doi:10.1002/cphc.201701223.
- [17] M. Happel, Y. Lykhach, N. Tsud, T. Skála, K.C. Prince, V. Matolín, J. Libuda, Mechanism of Sulfur Poisoning and Storage: Adsorption and Reaction of SO₂ with Stoichiometric and Reduced Ceria Films on Cu(111), J. Phys. Chem. C. 115 (2011) 19872–19882. doi:10.1021/jp207014z.

- [18] A. Beste, D.R. Mullins, S.H. Overbury, R.J. Harrison, Adsorption and dissociation of methanol on the fully oxidized and partially reduced (111) cerium oxide surface: Dependence on the configuration of the cerium 4f electrons, Surf. Sci. 602 (2008) 162– 175. doi:10.1016/j.susc.2007.10.024.
- [19] V. Matolín, J. Libra, M. Škoda, N. Tsud, K.C. Prince, T. Skála, Methanol adsorption on a CeO₂(111)/Cu(111) thin film model catalyst, Surf. Sci. 603 (2009) 1087–1092. doi:10.1016/j.susc.2009.02.010.
- [20] A. Neitzel, V. Johánek, Y. Lykhach, T. Skála, N. Tsud, M. Vorokhta, V. Matolín, J. Libuda, Reduction of Pt²⁺ species in model Pt–CeO₂ fuel cell catalysts upon reaction with methanol, Appl. Surf. Sci. 387 (2016) 674–681. doi:https://doi.org/10.1016/j.apsusc.2016.06.156.
- [21] Y. Lykhach, A. Neitzel, K. Ševčíková, V. Johánek, N. Tsud, T. Skála, K.C. Prince, V. Matolín, J. Libuda, The mechanism of hydrocarbon oxygenate reforming: C-C bond scission, carbon formation, and noble-metal-free oxide catalysts., ChemSusChem. 7 (2014) 77–81. doi:10.1002/cssc.201301000.
- [22] W.O. Gordon, Y. Xu, D.R. Mullins, S.H. Overbury, Temperature evolution of structure and bonding of formic acid and formate on fully oxidized and highly reduced CeO₂(111), Phys. Chem. Chem. Phys. 11 (2009) 11171–11183. doi:10.1039/B913310K.
- [23] Y. Lykhach, M. Happel, V. Johánek, T. Skála, F. Kollhoff, N. Tsud, F. Dvořák, K.C. Prince, V. Matolín, J. Libuda, Adsorption and Decomposition of Formic Acid on Model Ceria and Pt/Ceria Catalysts, J. Phys. Chem. C. 117 (2013) 12483–12494. doi:10.1021/jp311008v.
- [24] A. Neitzel, Y. Lykhach, V. Johánek, N. Tsud, T. Skála, K.C. Prince, V. Matolín, J. Libuda, Decomposition of Acetic Acid on Model Pt/CeO₂ Catalysts: The Effect of Surface Crowding J. Phys. Chem. C. 119 (2015) 13721-13734. doi:10.1021/acs.jpcc.5b03079.
- [25] F.C. Calaza, T.-L. Chen, D.R. Mullins, Y. Xu, S.H. Overbury, Reactivity and reaction intermediates for acetic acid adsorbed on CeO₂(111), Catal. Today. 253 (2015) 65–76. doi:https://doi.org/10.1016/j.cattod.2015.03.033.

- [26] C. Zhao, Y. Xu, Theoretical investigation of dephosphorylation of phosphate monoesters on CeO₂(111), Catal. Today. 312 (2018) 141–148. doi:https://doi.org/10.1016/j.cattod.2018.02.033.
- [27] D.A. Chen, J.S. Ratliff, X. Hu, W.O. Gordon, S.D. Senanayake, D.R. Mullins, Dimethyl methylphosphonate decomposition on fully oxidized and partially reduced ceria thin films, Surf. Sci. 604 (2010) 574–587. doi:10.1016/j.susc.2009.12.028.
- [28] J. Paier, C. Penschke, J. Sauer, Oxygen Defects and Surface Chemistry of Ceria: Quantum Chemical Studies Compared to Experiment, Chem. Rev. 113 (2013) 3949–3985. doi:10.1021/cr3004949.
- [29] J. Perdew, J. Chevary, S. Vosko, K. Jackson, M. Pederson, D. Singh, C. Fiolhais, Atoms, molecules, solids, and surfaces: Applications of the generalized gradient approximation for exchange and correlation, Phys. Rev. B. 46 (1992) 6671–6687. doi:10.1103/PhysRevB.48.4978.2.
- [30] M. Dion, H. Rydberg, E. Schröder, D.C. Langreth, B.I. Lundqvist, Van der Waals Density Functional for General Geometries, Phys. Rev. Lett. 92 (2004) 246401. https://link.aps.org/doi/10.1103/PhysRevLett.92.246401.
- [31] G. Román-Pérez, J.M. Soler, Efficient Implementation of a van der Waals Density Functional: Application to Double-Wall Carbon Nanotubes, Phys. Rev. Lett. 103 (2009) 096102. doi:10.1103/PhysRevLett.103.096102.
- [32] J. Klimeš, D.R. Bowler, A. Michaelides, Chemical accuracy for the van der Waals density functional, J. Phys. Condens. Matter. 22 (2010) 22201–22205. http://stacks.iop.org/0953-8984/22/i=2/a=022201.
- [33] J. Klimeš, D.R. Bowler, A. Michaelides, Van der Waals density functionals applied to solids, Phys. Rev. B. 83 (2011) 195131–19543. https://link.aps.org/doi/10.1103/PhysRevB.83.195131.
- [34] G. Kresse, J. Hafner, Ab initio molecular dynamics for liquid metals, Phys. Rev. B. 47 (1993) 558–561. doi:10.1103/PhysRevB.47.558.
- [35] G. Kresse, J. Hafner, Ab initio molecular-dynamics simulation of the liquid-metal-

- amorphous-semiconductor transition in germanium, Phys. Rev. B. 49 (1994) 14251–14269. doi:10.1103/PhysRevB.49.14251.
- [36] G. Kresse, J. Furthmüller, Efficiency of ab-initio total energy calculations for metals and semiconductors using a plane-wave basis set, Comput. Mater. Sci. 6 (1996) 15–50. doi:10.1016/0927-0256(96)00008-0.
- [37] G. Kresse, J. Furthmüller, Efficient iterative schemes for ab initio total-energy calculations using a plane-wave basis set, Phys. Rev. B. 54 (1996) 11169–11186. https://link.aps.org/doi/10.1103/PhysRevB.54.11169.
- [38] P.E. Blöchl, Projector augmented-wave method, Phys. Rev. B. 50 (1994) 17953–17979. doi:10.1103/PhysRevB.50.17953.
- [39] G. Kresse, D. Joubert, From ultrasoft pseudopotentials to the projector augmented-wave method, Phys. Rev. B. 59 (1999) 1758–1775. https://link.aps.org/doi/10.1103/PhysRevB.59.1758.
- [40] J. Neugebauer, M. Scheffler, Adsorbate-substrate and adsorbate-adsorbate interactions of Na and K adlayers on Al(111), Phys. Rev. B. 46 (1992) 16067–16080. https://link.aps.org/doi/10.1103/PhysRevB.46.16067.
- [41] H.J. Monkhorst, J.D. Pack, Special points for Brillouin-zone integrations, Phys. Rev. B. 13 (1976) 5188–5192. doi:10.1103/PhysRevB.13.5188.
- [42] S.L. Dudarev, G.A. Botton, S.Y. Savrasov, C.J. Humphreys, A.P. Sutton, Electron-energy-loss spectra and the structural stability of nickel oxide: An LSDA+U study, Phys. Rev. B. 57 (1998) 1505–1509. doi:10.1103/PhysRevB.57.1505.
- [43] L. Gerward, J.S. Olsen, Powder diffraction analysis of cerium dioxide at high pressure, Powder Diffr. 8 (1993) 127–129. doi:10.1017/S0885715600017966.
- [44] L. Gerward, J. Staun Olsen, L. Petit, G. Vaitheeswaran, V. Kanchana, A. Svane, Bulk modulus of CeO₂ and PrO₂—An experimental and theoretical study, J. Alloys Compd. 400 (2005) 56–61. doi:10.1016/j.jallcom.2005.04.008.
- [45] M. Hanus, M. Kabeláč, J. Rejnek, F. Ryjáček, P. Hobza, Correlated ab Initio Study of Nucleic Acid Bases and Their Tautomers in the Gas Phase, in a Microhydrated

- Environment, and in Aqueous Solution. Part 3. Adenine, J. Phys. Chem. B. 108 (2004) 2087–2097. doi:10.1021/jp036090m.
- [46] J.J. Yeh, I. Lindau, Atomic subshell photoionization cross sections and asymmetry parameters: $1 \le Z \le 103$, At. Data Nucl. Data Tables. 32 (1985) 1–155. doi:https://doi.org/10.1016/0092-640X(85)90016-6.
- [47] D.N. Kelly, C.P. Schwartz, J.S. Uejio, A.M. Duffin, A.H. England, R.J. Saykally, Communication: Near edge x-ray absorption fine structure spectroscopy of aqueous adenosine triphosphate at the carbon and nitrogen K-edges., J. Chem. Phys. 133 (2010) 101103–101107. doi:10.1063/1.3478548.
- [48] Y. Zubavichus, A. Shaporenko, V. Korolkov, M. Grunze, M. Zharnikov, X-ray absorption spectroscopy of the nucleotide bases at the carbon, nitrogen, and oxygen K-edges, J. Phys. Chem. B. 112 (2008) 13711–13716. doi:10.1021/jp802453u.
- [49] K. Momma, F. Izumi, VESTA 3 for three-dimensional visualization of crystal, volumetric and morphology data, J. Appl. Crystallogr. 44 (2011) 1272–1276. doi:10.1107/S0021889811038970.
- [50] R.E.A. Kelly, W. Xu, M. Lukas, R. Otero, M. Mura, Y.-J. Lee, E. Laegsgaard, I. Stensgaard, L.N. Kantorovich, F. Besenbacher, An investigation into the interactions between self-assembled adenine molecules and a Au(111) surface, Small. 4 (2008) 1494–500. doi:10.1002/smll.200800172.
- [51] R. Otero, W. Xu, M. Lukas, R.E.A. Kelly, E. Lægsgaard, I. Stensgaard, J. Kjems, L.N. Kantorovich, F. Besenbacher, Specificity of Watson-Crick base pairing on a solid surface studied at the atomic scale, Angew. Chemie Int. Ed. 47 (2008) 9673–9676. doi:10.1002/anie.200803333.
- [52] M. Lukas, R.E.A. Kelly, L.N. Kantorovich, R. Otero, W. Xu, E. Laegsgaard, I. Stensgaard, F. Besenbacher, Adenine monolayers on the Au(111) surface: structure identification by scanning tunneling microscopy experiment and ab initio calculations., J. Chem. Phys. 130 (2009) 024705. doi:10.1063/1.3046690.
- [53] C. Yang, X. Yu, S. Heißler, P.G. Weidler, A. Nefedov, Y. Wang, C. Wöll, T. Kropp, J. Paier, J. Sauer, O2 Activation on Ceria Catalysts—The Importance of Substrate

- Crystallographic Orientation, Angew. Chemie Int. Ed. 56 (2017) 16399–16404. doi:10.1002/anie.201709199.
- [54] P.A. Redhead, Thermal desorption of gases, Vacuum. 12 (1962) 203–211. doi:https://doi.org/10.1016/0042-207X(62)90978-8.
- [55] W. Tang, E. Sanville, G. Henkelman, A grid-based Bader analysis algorithm without lattice bias, J. Phys. Condens. Matter. 21 (2009) 084204. doi:10.1088/0953-8984/21/8/084204.
- [56] M. Buchholz, M. Xu, H. Noei, P. Weidler, A. Nefedov, K. Fink, Y. Wang, C. Wöll, Interaction of carboxylic acids with rutile TiO₂(110): IR-investigations of terephthalic and benzoic acid adsorbed on a single crystal substrate, Surf. Sci. 643 (2016) 117–123. doi:https://doi.org/10.1016/j.susc.2015.08.006.